iJRASET
International Journal For Research in Applied Science and Engineering Technology

INTERNATIONAL JOURNAL FOR RESEARCH

IN APPLIED SCIENCE & ENGINEERING TECHNOLOGY

Volume: 14 **Issue:** IV **Month of publication:** April 2026

DOI: https://doi.org/10.22214/ijraset.2026.79816

www.ijraset.com

Call: 08813907089 | E-mail ID: ijraset@gmail.com

International Journal for Research in Applied Science & Engineering Technology (IJRASET)
ISSN: 2321-9653; IC Value: 45.98; SJ Impact Factor: 7.538
Volume 14 Issue IV Apr 2026- Available at www.ijraset.com

Multi-Class Brain Tumor Classification from MRI Using ResNet50V2 Transfer Learning with Two-Stage Augmentation, Grad-CAM Explainability, and Cross-Dataset Validation

Shalma Muji M[1], Nithin T[2], Lavanya D[3], Abhiram VS[4], S Sreeja[5], A Kousalya[6]
[1, 2, 3, 4]B.Tech Student, [5]M.E Student, [6]Associate Professor Department of Artificial Intelligence and Data Science United Institute of Technology, Coimbatore, Tamil Nadu, India

Abstract: ***Brain tumor classification from magnetic resonance imaging (MRI) remains a challenging clinicaltaskduetointer-classvisualsimilarityandsignificantvari-ation across imaging protocols and acquisition equipment.Accurate and timely classification of glioma, meningioma, pituitary tumor, and normal brain tissue is critical for treatment planning and patient outcomes.This work proposes a two-phase transfer learning framework based on ResNet50V2 pretrained on ImageNetfor four-class brain MRI classification.A two-stage augmentation pipeline combin-ingofflinedegradationaugmentationGaussiannoise(SNR=18.39dB),Gaussianblur(SSIM≥0.93),andresolutiondegradation(SSIM≥0.85)—withonlinegeometric augmentation was employed to improve cross-scanner robustness. Class imbalance was addressed through balanced class weighting.Grad-CAM visualisa-tions were generated to provide anatomically interpretable explanations of model decisions.Evaluated on a held-out test set of 310 images from the Daneshmand dataset, the proposed model achieved 89.68% accuracy, Cohen's κ=0.8595, and macro-AUCof0.9820. ExternalvalidationontheindependentCE-MRIdataset (n=394)yielded84.52%accuracyandmacro-AUCof0.9729, withMcNemar's test confirming no statistically significant difference in error patterns (p=0.1882), demonstrating consistent cross-dataset generalisation. Grad-CAM activations con-firmed anatomically consistent focus across all four classes, supporting clinical in-terpretability.The complete implementation is publicly available at the project repository.***

Keywords: Brain tumor classification, magnetic resonance imaging, transfer learning, ResNet50V2, Grad-CAM, convolutional neural networks, medical image analysis, deep learning.

I. INTRODUCTION

Brain tumors represent one of the most life-threatening neurological conditions, with primary central nervous system tumors accounting for approximately 308,102 new cases and251,329deathsgloballyin2020[1]. Amongthemostprevalentprimary braintumors,gliomasaccountfornearly80%ofmalignantcases,whilemeningiomasrepresentthemost common benign intracranial tumors [2].Accurate and early classification of tumor type is critical, as treatment protocols differ fundamentally across tumor categories [3].

Magnetic resonance imaging (MRI) remains the gold standard for brain tumor diagnosis duetoitssuperior softtissuecontrastandabsenceofionisingradiation.However,manual interpretation of MRI scans by radiologists is time-consuming, subject to inter-observer variability, and increasingly strained by growing imaging volumes in clinical settings.

A. ClinicalMotivationandProblemSignificance

The visual similarity between tumor classes presents a fundamental challenge for auto-mated classification.Gliomas, which originate within brain parenchyma, share overlap-ping intensity distributions with meningiomas, which arise from the meningeal lining. Furthermore,thescarcityoflargeannotatedmedicalimagingdatasetsandtheinher-ent class imbalance between tumor subtypes compound the difficulty of training robust classifiers. Clinicaldeploymentadditionallydemandscross-scannergeneralisation—the ability to maintain diagnostic accuracy across images acquired from different MRI ma-chines, field strengths, and acquisition protocols.

B. LimitationsofExistingApproaches

Existing deep learning approaches suffer from several limitations.First, the majority of published work evaluates models exclusively on single-source datasets [4].Second, few studies incorporate quantified augmentation quality metrics to validate clinical plausi-bility[5].Third, explainability is frequently neglected.Fourth, class imbalance is often unaddressed.

C. ContributionsofThisWork

Thispaperaddressestheselimitationsthroughthefollowingcontributions:

1) Atwo-phasetransferlearningstrategyusingResNet50V2achieving89.68%accu-racyandmacro-AUCof0.9820onastrictlyheld-outtestsetof310images.
2) A two-stage augmentation pipeline with quantitative quality validation using SNR, PSNR,andSSIMmetricsconfirmingallaugmentedsamplesmaintainSSIM≥0.85.
3) Cross-datasetgeneralisationevaluatedontheindependent CE-MRIbenchmark (n=394) achieving 84.52% accuracy and macro-AUC of 0.9729 without retrain-ing, with McNemar's test confirming consistent generalisation (p=0.1882).
4) Grad-CAMvisualisations demonstrating anatomicallyconsistentmodelattention across all four classes.
5) Balancedclassweightingcorrectingforthe2.08×classimbalanceratiowithclinical priority assigned to minimising false positive tumor predictions.

Thecompleteimplementationispubliclyavailableat[19].

II. RELATED WORK

A. TraditionalMachineLearningApproaches

Earlysystemsreliedonhand-craftedfeaturesandclassicalclassifiers.Chengetal.[6]pro-posed augmentation-based feature extraction achieving 84.19% accuracy on a four-class datasetusingbag-of-wordsrepresentationswith SVMclassification. Whiledemonstrating feasibility, reliance on manually engineered features limited generalisation.

B. CNN-BasedClassificationMethods

Abiwinandaetal.[7]demonstratedthatasimpleCNNarchitecturecouldachievecompet-itive performance without hand-crafted features, reporting 84.19% accuracy on a three-class dataset.Pashaei et al. [8] explored compact CNN architectures achieving 93.68% accuracy on binary tasks but noting reduced performance on multi-class problems.

C. TransferLearningforMedicalImaging

Deepak and Ameer [9] applied GoogLeNet transfer learning reporting 92.12% accuracy on a three-class problem.Khan et al. [10] compared multiple pretrained architectures with ResNet-based models consistently outperforming alternatives.Rehman et al. [11] achieved 95.00% using fine-tuned VGG19 on a three-class dataset without external vali-dation. Sultan et al. [12] achieved 96.56% on binary classification, though binary formu-lations fail to address the clinically critical distinction between tumor subtypes.

D. ResearchGapsAddressedbyThisWork

The present work addresses:single-source evaluation, lack of quantified augmentation validation, inconsistent imbalance handling, and absent explainability.A comparison against prior work is presented in Table 8.

‘

III. DATASET AND PREPROCESSING

A. PrimaryDataset—DaneshmandBrainMRI

The primary dataset is the Brain MRI Images for Brain Tumor Detection dataset [13] comprising3,096T1-weightedMRIimages:gliomatumor(901,29.1%),meningiomatumor(913,29.5%),normalbrain(438,14.1%),andpituitarytumor(844,27.3%).Allimagesareuniformlysizedat256×256pixelsinRGBformatwithzerocorruptedfilesconfirmed.Per-class mean pixel intensitieswere computed as:

$$\bar{I}_c = \frac{1}{N_c} \sum_{i=1}^{N_c} \mu(I_c)_i \qquad (1)$$

(where $\bar{I}_c$ is the mean intensity for class c, N_c is the number of images in class c, and $\mu(I^c)$ is the mean pixel value of the i-th image. This yielded: glioma (47.41±10.71), meningioma (57.50±14.58), normal (62.51±20.97), and pituitary (51.76±8.37). The class distribution is illustrated in Fig. 1 and representative samples in Fig. 2.

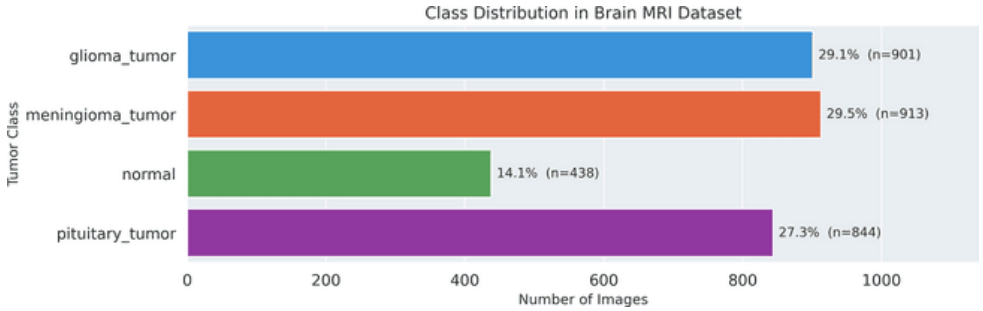

Figure 1: Class distribution of the Daneshmand Brain MRI dataset. Meningioma is most represented (29.5%) and normal least represented (14.1%), yielding an imbalance ratio of 2.08×.

B. External Validation Dataset—CE-MRI

The CE-MRI Brain Tumor Classification dataset [14] was employed exclusively for ex-ternal validation comprising 394 test images: glioma (100), meningioma (115), normal (105), pituitary (74). No CE-MRI images were used during training or validation.

C. Data Partitioning and Leakage Prevention

Stratified splitting yielded: 72% training (2,228 images), 18% validation (558), 10% held-out test (310). Zero overlapping files were reconfirmed across all split pairs through explicit filepath intersection checks. The split distribution is summarised in Table 1 and illus-trated in Fig. 3.

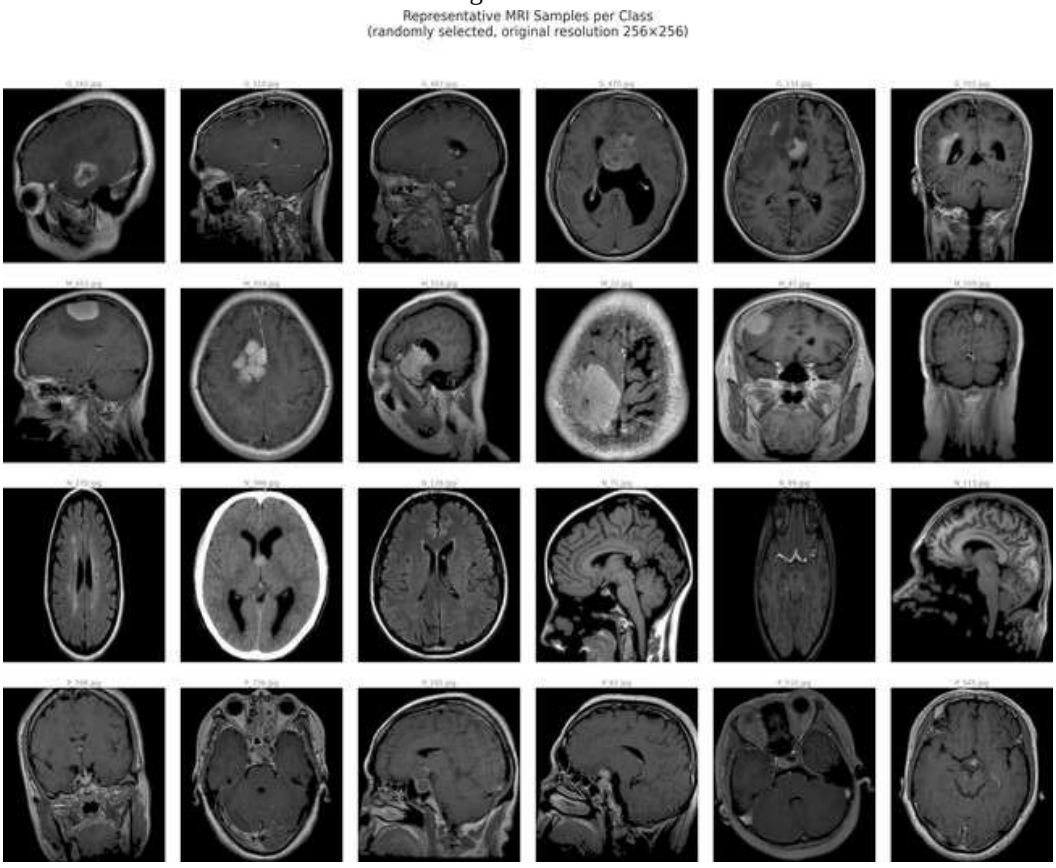

Figure 2: Representative MRI samples per class from the Daneshmand dataset. Six randomly selected images shown per class at original 256×256 resolution.

Table1:DatasetSplitStatistics

Split	Total	Glioma	Mening.	Normal	Pituit.
Training	2,228	649	657	315	607
Validation	558	162	165	79	152
Test	310	90	91	44	85
Total	3,096	901	913	438	844

D. ClassImbalanceAnalysis

A 2.08×class imbalance ratio was observed between the most represented class (menin-gioma, 913) and least represented (normal, 438).t-SNE visualisation of raw pixel fea-turesinFig.4confirmedsubstantialinter-classoverlap,motivatingdeeptransferlearning.

Pixelintensitydistributionsareshowninfig.5.

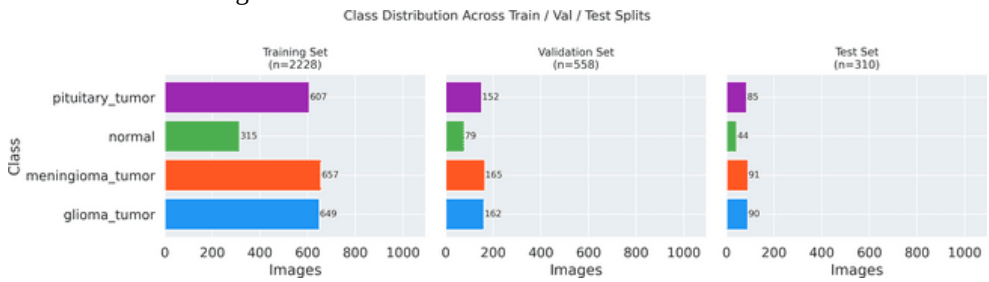

Figure 3:Class distribution across training, validation, and test splits.Stratified splitting maintained class proportions within ±0.2% across all partitions.

IV. METHODOLOGY

A. Two-StageAugmentationPipeline

A two-stage augmentation strategy was designed to simulate realistic MRI acquisition variability while preserving clinically relevant structural features.

Stage 1 — Offline degradation augmentation expanded the training set from 2,228 to 4,456 images (2.00× increase) through three degradation methods applied in random combinations:

Gaussiannoisewithμ=0andσ=10wasappliedas:

$$I_{noisy}(x, y) = \text{clip}\{I(x, y) + N(0, \sigma^2), 0, 255\} \quad (2)$$

yieldingSNR=18.39dB,withintheclinicallyacceptablerangeof10–30dBfordiagnostic MRI.

Gaussianblurwithkernel sizes$k \in \{3,5,7\}$wasappliedas:

$$I_{blur}(x,y)=G_k(i,j)\cdot I(x-i,y-j) \quad (3)$$

i,j

where$G_k$istheGaussiankernelofsize$k$,achievingSSIMscoresof0.9818,0.9622,and 0.9312 respectively.

Resolutiondegradationthroughdownsample-upsamplecyclesatscalefactors$s \in$ [0.30,0.70]:

$$I_{deg}=UD(I,s),W,H \quad (4)$$

where D downsamples using INTER AREA and U upsamples using INTER LINEAR back to original dimensions (W,H), achieving PSNR=30.87–38.13dB and SSIM=0.8954–0.9784.Allaugmented samples maintained SSIM≥0.85, confirming clinical plausibility. Augmentation quality metrics are summarised in Table 2 and visualised in Figs. 6 and 7.

Stage 2 — Online geometric augmentation applied rotation (±20°), width and height shifts (±10%), zoom (±10%), and horizontal flipping dynamically during training.

B. ModelArchitecture

ResNet50V2 [15] pretrained on ImageNet was employed as the backbone.The base model comprises190layerswith23.56Mparametersproducinga7×7×2048featuremapfrom

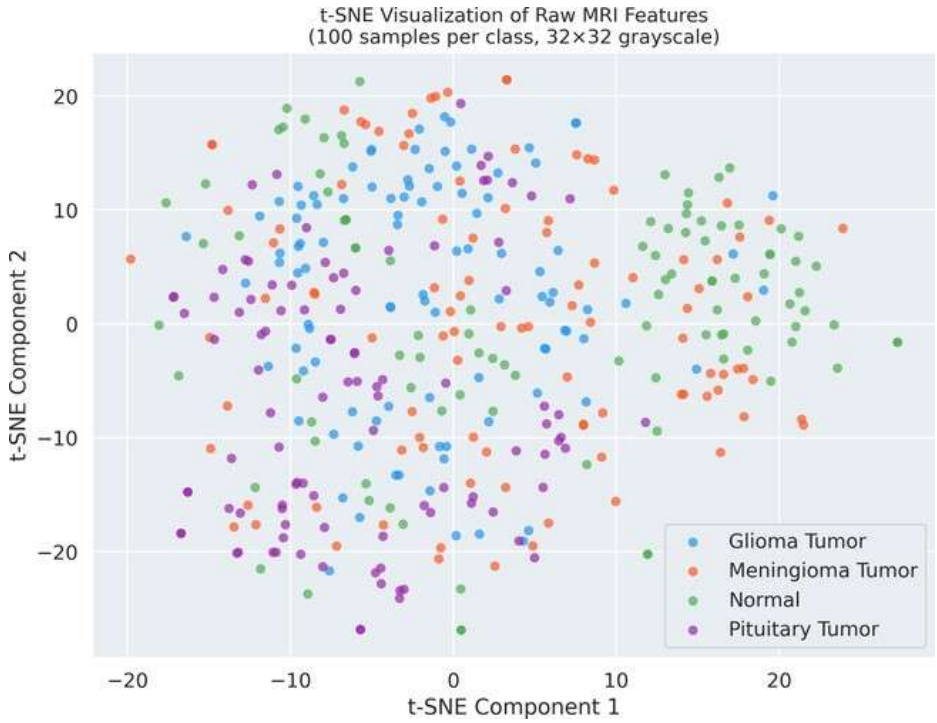

Figure 4:t-SNE of raw pixel features (100 samples per class, 32×32 grayscale).Significant inter-class overlap confirms shallow approaches are insufficient, motivating deep transfer learning.

224×224×3inputs.Acustomclassificationheadwasappended:

$$\hat{y} = \mathrm{softmax}\big(W_2 \cdot \mathrm{dropout}\big(\mathrm{ReLU}\big(W_1 \cdot \mathrm{GAP}(\mathbf{F}) + b_1\big)\big) + b_2\big) \quad (5)$$

where$\mathbf{F} \in \mathbb{R}^{7\times7\times2048}$is thebackbonefeaturemap, GAPdenotesglobal averagepooling, $W_1 \in \mathbb{R}^{1024\times2048}andW_2 \in \mathbb{R}^{4\times1024}$arelearnableweightmatrices,anddropoutrate=0.5. Totalparameters:25,675,268with2,106,372trainableinPhase1.

C. Two-PhaseTransferLearning

*Phase 1 — Frozen base:*All 190 ResNet50V2 layers were frozen.The Adam optimiser[17]withlearningrate$lr_1=1\times10^{-4}$was used with early stopping (patience=15) and Re-duceLROnPlateau(factor=0.5,patience=3).Phase1convergedatepoch17withbest validation accuracy 90.86% and AUC 0.9871 in 29.4min on a Tesla P100-PCIE-16GB GPU.

*Phase2—Fine-tuning:*Thetop30layers(entireconv5block:conv5_block1,conv5_block2, conv5_block3, and post_bn) were unfrozen for domain-specific adaptation.The modelwasrecompiledwith Adamatreduced learningrate$lr_2=1\times10^{-5}$toprevent catastrophicforgetting.Phase2trainedforall20epochsachievingbestvalidationaccuracy91.04%andAUC0.9878in19.4min.Totaltrainingtime:48.8min.Learningcurvesarepresented in Fig. 10.

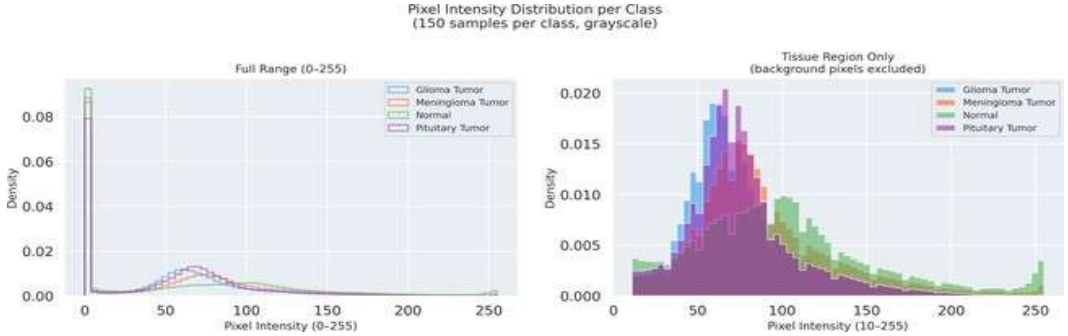

Figure 5: Pixel intensity distribution per class. Left: full range (0–255). Right: tissue regiononly(pixels>10).Glioma and meningioma exhibit overlapping distributions con-sistent with their high misclassification rate.

Table2:AugmentationQualityMetrics

Method	Parameter	SNR(dB)	PSNR(dB)	SSIM
GaussianNoise	μ=0,σ=10	18.39	—	—
GaussianBlur	k=3×3	—	36.80	0.9794
GaussianBlur	k=5×5	—	32.79	0.9519
GaussianBlur	k=7×7	—	29.39	0.9050
Low Res	scale=70%	—	35.85	0.9747
Low Res	scale=50%	—	32.70	0.9497
Low Res	scale=30%	—	27.08	0.8543

D. ClassImbalanceCorrection

Balancedclassweightswerecomputedas:

$$w_i = \frac{N}{K \cdot n_i} \quad (6)$$

where$N$istotaltrainingsamples,K=4isthenumberofclasses,and$n_i$isthenumber ofsamplesinclass i.This yielded:w_{glioma}=0.859, $w_{\text{meningioma}}$=0.848, w_{normal}=1.767, $w_{\text{pituitary}}$=0.917.The elevated weight for the normal class ensures misclassification of healthy brain tissue is penalised approximately twice as heavily as misclassification of majority tumor classes.

E. Grad-CAMExplainability

Gradient-weighted Class Activation Mapping (Grad-CAM) [16] generates spatially lo-calised explanations by computing:

$$\alpha_k^c = \frac{1}{Z}\sum_i \sum_j \frac{\partial y^c}{\partial A_{ij}^k} \quad (7)$$

whereα_k^cistheimportanceweightoffeaturemap$k$forclass$c$,y^cistheclassscore,andA_{ij}^kisthe(i,j)activationofthe$k$-thfeaturemap.Theclass-discriminativelocalisation
mapisthen:

$$L_{\text{Grad-CAM}}^c = \text{ReLU}\left(\sum_k \alpha_k^c A^k\right) \quad (8)$$

Gradientswereextractedatconv5_block3_outandheatmapsupsampledto224×224 via bicubic interpolation with overlay parameter α =0.4.Average Grad-CAM heatmapswerecomputedacross20samplesperclass.

V. EXPERIMENTAL RESULTS

A. Implementation Details

All experiments used TensorFlow 2.19.0, Keras 3.13.2, NumPy 2.0.2, OpenCV 4.12.0, scikit-learn1.6.1,Python3.12.12onaTeslaP100-PCIE-16GB(15,511MB)GPU.Mixed precision (float16/float32) was enabled.Random seed 42 was applied across NumPy, TensorFlow, and Python.All hyperparameters are consolidated in Table 3.

Table3:HyperparameterConfiguration

Hyperparameter	Value
Inputimagesize	224×224×3
Batchsize	32
Phase1learningrate	1×10^{-4}

Phase2learningrate	1×10^{-5}
Fine-tunedlayers	30(conv5block)
Dropoutrate	0.5
Denseunits	1,024
MaxepochsPhase1	50
MaxepochsPhase2	20
Earlystoppingpatience	15
ReduceLROnPlateaupatience	3
LRreductionfactor	0.5
MinimumLR	1×10^{-6}
Randomseed	42
GPU	TeslaP100-PCIE-16GB

B. InternalTestSetPerformance

The proposed model achieved 89.68% accuracy, Cohen's κ=0.8595 indicating almost perfect agreement [18], and macro-AUC of 0.9820 on the strictly held-out test set of 310 images.The confusion matrix is presented in Fig. 11 and per-class classification results in Table 4.

Table4:ClassificationReport—InternalTestSet(n=310)

Class	Precision	Recall	F1	Support
Glioma	0.9277	0.8556	0.8902	90
Meningioma	0.8462	0.8462	0.8462	91
Normal	0.9773	0.9773	0.9773	44
Pituitary	0.8804	0.9529	0.9153	85
Macroavg	0.9079	0.9080	0.9072	310
Weightedavg	0.8972	0.8968	0.8958	310

C. Per-ClassClinicalMetrics

Sensitivity,specificity,positivepredictivevalue(PPV),andnegativepredictivevalue (NPV) were computed as:

$$\text{Sensitivity}=\frac{TP}{TP+FN} \quad (9)$$

$$\text{Specificity}=\frac{TN}{TN+FP} \quad (10)$$

$$\text{PPV}=\frac{TP}{TP+FP} \quad (11)$$

$$\text{NPV}=\frac{TN}{TN+FN} \quad (12)$$

ResultsarepresentedinTable5andFig.12.Thenormalclassachievedsensitivityof 0.9773, specificity of 0.9962, and NPV of 1.0000.

Table5:Per-ClassClinicalMetrics—InternalTestSet

Class	Sensitivity	Specificity	PPV	NPV
Glioma	0.8556	0.9727	0.9277	0.9427
Meningioma	0.8462	0.9361	0.8462	0.9361
Normal	0.9773	0.9962	0.9773	0.9962
Pituitary	0.9529	0.9511	0.8804	0.9817

D. ROCAnalysisandAUCConfidenceIntervals

ROC curves were computed using the one-versus-rest strategy.The AUC for each class was computed as:

$$AUC = \int_0^1 TPR(FPR^{-1}(t))dt \quad (13)$$

Bootstrapconfidenceintervalswereestimatedover1,000iterations.ResultsareinTable6andFig.15.ThemacroaverageAUCof0.9820 confirmsstrongdiscriminativecapability across all four classes.

Table6:AUCwith95%BootstrapConfidenceIntervals

Class	Int.AUC	95%CI	Ext.AUC	95%CI
Glioma	0.9651	[0.9369–0.9863]	0.9589	[0.9384–0.9763]
Meningioma	0.9710	[0.9546–0.9849]	0.9639	[0.9401–0.9826]
Normal	0.9975	[0.9920–1.0000]	0.9792	[0.9673–0.9888]
Pituitary	0.9937	[0.9876–0.9983]	0.9901	[0.9829–0.9954]
Macroavg	0.9820	—	0.9729	—

E. ExternalValidation—CE-MRIDataset

Withoutretraining,themodelachieved84.52%accuracy, κ=0.7903, andmacro-AUCof 0.9729ontheCE-MRIdataset.TheconfusionmatrixandROCcurvesarepresented in Figs. 19 and 20.The macro-AUC degradation was only 0.0091, indicating that dis-criminative ranking capability generalises substantially better than absolute classification accuracy across imaging sources.

F. StatisticalSignificanceTesting

McNemar'stestwasappliedtoassesswhethererrorpatternsdifferedsignificantlybetweeninternalandexternalvalidationsets.Thetests tatisticis:

$$\chi^2 = \frac{(b-c)^2 b}{+c} \quad (14)$$

where*b* and *c* denote discordant prediction pairs.The test yielded p=0.1882, confirm-ing*no statistically significant difference* in error patterns between datasets.This result validates that the model generalises consistently across independent imaging sources.

An independent samples t-test comparing Phase 1 and Phase 2 validation accuracies yielded p=0.5954, indicating stable convergence across both training phases without statistically significant deviation.

BootstrapAUCconfidenceintervalsarepresentedinTable6.Theoverlappingconfidence intervals between internal and external AUC values for all classes provide statistical evidence of cross-dataset generalisation.

G. AblationStudy

ProgressiveevaluationresultsaresummarisedinTable7andFig.21.

H. ComparisonwithPriorWork

Table 8 compares the proposed method against representative prior works.The proposed frameworkuniquelyincorporatesexternalcross-datasetvalidation—acriticalevaluation criterion absent from all compared methods.

Table7:AblationStudy—ProgressiveEvaluation

Configuration	ValAcc	ValAUC	TestAcc	κ
Phase1frozenbase	90.86%	0.9871	—	—
Phase2fine-tuned	91.04%	0.9878	—	—
Finalinternaltest	—	—	89.68%	0.8595
FinalCE-MRIexternal	—	—	84.52%	0.7903

Table8:ComparisonwithPriorWork

Method	Architecture	Cls	Accuracy	Ext.Val
Chengetal.[6]	SVM+BoW	4	84.19%	No
Abiwinandaetal.[7]	CNN	3	84.19%	No
Deepak&Ameer[9]	GoogLeNet	3	92.12%	No
Khanetal.[10]	ResNet50	4	90.67%	No
Rehmanetal.[11]	VGG19	3	95.00%	No
Sultanetal.[12]	CNN	2	96.56%	No
Proposed	**ResNet50V2**	**4**	**89.68%**	**Yes**

VI. DISCUSSION

A. *ErrorAnalysis—Glioma-MeningiomaConfusion*

The most frequent misclassification involved glioma-meningioma confusion:10 of 32 in-ternalerrorsand12of61externalerrors.Thisreflectsoverlappingintensityprofilesin plain T1-weighted MRI as demonstrated by Fig. 5 and the t-SNE comparison in Fig. 17. Grad-CAM in Fig. 16 confirms the model implicitly learned the intrinsic versus extrinsic tumor location distinction, with glioma activations concentrated in cerebral hemispheretissueandmeningiomaactivationshighlightingperipheralbrainsurfaces.However,ab-sence of contrast enhancement limits full exploitation of anatomical cues such as the duraltail sign.

B. *DomainShiftandCross-DatasetGeneralisation*

The5.16percentagepointaccuracyreductionfrominternal(89.68%)toexternal(84.52%) validation reflects modest domain shift between the Daneshmand and CE-MRI datasets. Crucially, McNemar'stestconfirmednostatisticallysignificant differenceinerrorpatterns (p=0.1882), validating consistent generalisation across imaging sources.The macro-AUC degradation of only 0.0091 further confirms that discriminative ranking capability is largely preserved across datasets.

C. *Grad-CAMClinicalInterpretability*

Grad-CAM confirmed anatomically consistent attention across all four classes as shown inFigs.16and18:gliomaactivationsincerebralhemispheres,meningiomaatperipheralsurfaces,pituitaryatthesellaturcica,andnormal scanswithdiffuseunfocusedactivation. AverageGrad-CAMheatmapsacross20samplesperclassconfirmedconsistencyofthese patterns, providing evidence that the model learned clinically meaningful discriminative features rather than spurious image artifacts.

D. *Limitations*

Key limitations include: 2D slice inputs precluding inter-slice spatial context; plain T1-weighted MRI without contrast enhancement limiting access to features such as the dural tail sign; single-institution training data; and absence of prospective clinical validation.

VII. CONCLUSION

A. *SummaryofContributions*

AtwophaseResNet50V2transferlearningframeworkwaspresentedforfourclassbrainMRItumorclassification,achieving89.68%accuracy, κ=0.8595, andmacro-AUC0.9820 on a strictly held-out internal test set. External validation on the independent CE-MRI benchmarkachieved84.52%accuracyandmacroAUC0.9729,withMcNemar'stestconfirmingnostatisticallysignificantdifferenceinerrorpatterns(p=0.1882), demonstrating consistent cross-dataset generalisation.Five principal contributions were demonstrated: quantitatively validated two-stage augmentation with mathematical formulation, two-phase transfer learning with progressive fine-tuning, balanced class weighting, anatomi-cally consistent Grad-CAM explainability with formal derivation, and statistically vali-dated external cross-dataset generalisation.

B. *Future Work*

Futuredirectionsinclude:multi-sourcetrainingdatacombiningbothdatasetpartitions toreducedomainshift;ananatomy-aware Bayesianconfidencefusion moduleforglioma-meningioma disambiguation; extension to 3D volumetric MRI; contrast-enhanced se-quence incorporation; and prospective multi-institution clinical validation.
The complete implementation is available at:https://www.kaggle.com/code/shalmamuji/mri-brain-tumor-classification

C. *Acknowledgment*

The authors thank Dr A Kousalya, Associate Professor, Department of Artificial Intelli-genceandDataScience, UnitedInstituteofTechnology, Coimbatore, TamilNadu, India, for mentorship and guidance throughout this work.

REFERENCES

[1] D. N. Louis et al., "The 2021 WHO Classification of Tumors of the Central Nervous System:asummary,"Neuro-Oncology,vol.23,no.8,pp.1231–1251,2021.
[2] Q.T.Ostrometal.,"CBTRUSStatisticalReport:PrimaryBrainandOtherCen-tral Nervous System Tumors Diagnosed in the United States in 2014–2018," Neuro-Oncology, vol. 23, no. S3, pp. iii1–iii105, 2021.
[3] D. N. Louis et al., "The 2016 World Health Organization Classification of Tumors ofthe Central Nervous System," Acta Neuropathologica, vol. 131, no. 6, pp. 803–820, 2016.
[4] A. Salehi, A. Ahmadi, and I. Heidari, "A brief survey on deep learning based brain tumor detection," arXiv preprint arXiv:2007.01169, 2020.
[5] C. Shorten and T. M. Khoshgoftaar,"A survey on image data augmentation fordeep learning," Journal of Big Data, vol. 6, no. 1, pp. 1–48, 2019.
[6] J.Chengetal.,"Enhancedperformanceofbraintumorclassificationviatumor regionaugmentationandpartition,"PLOSONE,vol.10,no.10,p.e0140381,2015.
[7] N.Abiwinanda,M.Hanif,S.T.Hesaputra,A.Handayani,andT.R.Mengko,"Brain tumorclassificationusingconvolutionalneuralnetwork,"inWorldCongressonMed-ical Physics and Biomedical Engineering, Singapore:Springer, 2019, pp. 183–189.
[8] A. Pashaei, H. Sajedi, and N. Jazayeri, "Brain tumor classification via convolutional neural network and extreme learning machines," in Proc. 8th Int. Conf. Computer and Knowledge Engineering (ICCKE), 2018, pp. 314–319.
[9] S.DeepakandP.M.Ameer,"BraintumorclassificationusingdeepCNNfeatures via transfer learning,"ComputersinBiologyandMedicine,vol. 111,p. 103345,2019.
[10] M. A. Khan et al., "Brain tumor detection and classification using MRI: a cross-sectional study," Computational and Mathematical Methods in Medicine, vol. 2020,
[11] p.6276735,2020.
[12] A. Rehman, S. Naz, M. I. Razzak, F. Akram, and M. Imran, "A deep learning-based framework for automatic brain tumor classification using transfer learning," Circuits, Systems,andSignalProcessing,vol.39,no.2,pp.757–775,2020.
[13] H. H. Sultan, N. M. Salem, and W. Al-Atabany, "Multi-classification of brain tumor imagesusingdeepneuralnetwork,"IEEEAccess,vol.7,pp.69215–69225,2019.
[14] S.Daneshmand,"BrainMRIImagesforBrainTumorDetection,"Kaggle,2020. [Online]. Available: https://www.kaggle.com/datasets/susandaneshmand/mri-images
[15] S.Chakrabarty,"BrainTumorClassification(MRI),"Kaggle,2019.[On-line].Available: https://www.kaggle.com/datasets/sartajbhuvaji/brain-tumor-classification-mri
[16] K.He, X.Zhang, S.Ren, andJ.Sun, "Identitymappingsindeepresidualnetworks," in Proc. ECCV, Amsterdam, 2016, pp. 630–645.
[17] R.R.Selvarajuetal.,"Grad-CAM:Visualexplanationsfromdeepnetworksvia gradient-based localization," in Proc. ICCV, Venice, 2017, pp. 618–626.
[18] D.P.KingmaandJ.Ba,"Adam:Amethodforstochasticoptimization,"inProc. ICLR, 2015.
[19] J. R. Landis and G. G. Koch, "The measurement of observer agreement for categor-ical data," Biometrics, vol. 33, no. 1, pp. 159–174, 1977.
[20] S.Muji,"MRIBrainTumorClassification,"Kaggle,2025.[Online].Available:https://www.kaggle.com/code/shalmamuji/mri-brain-tumor-classification

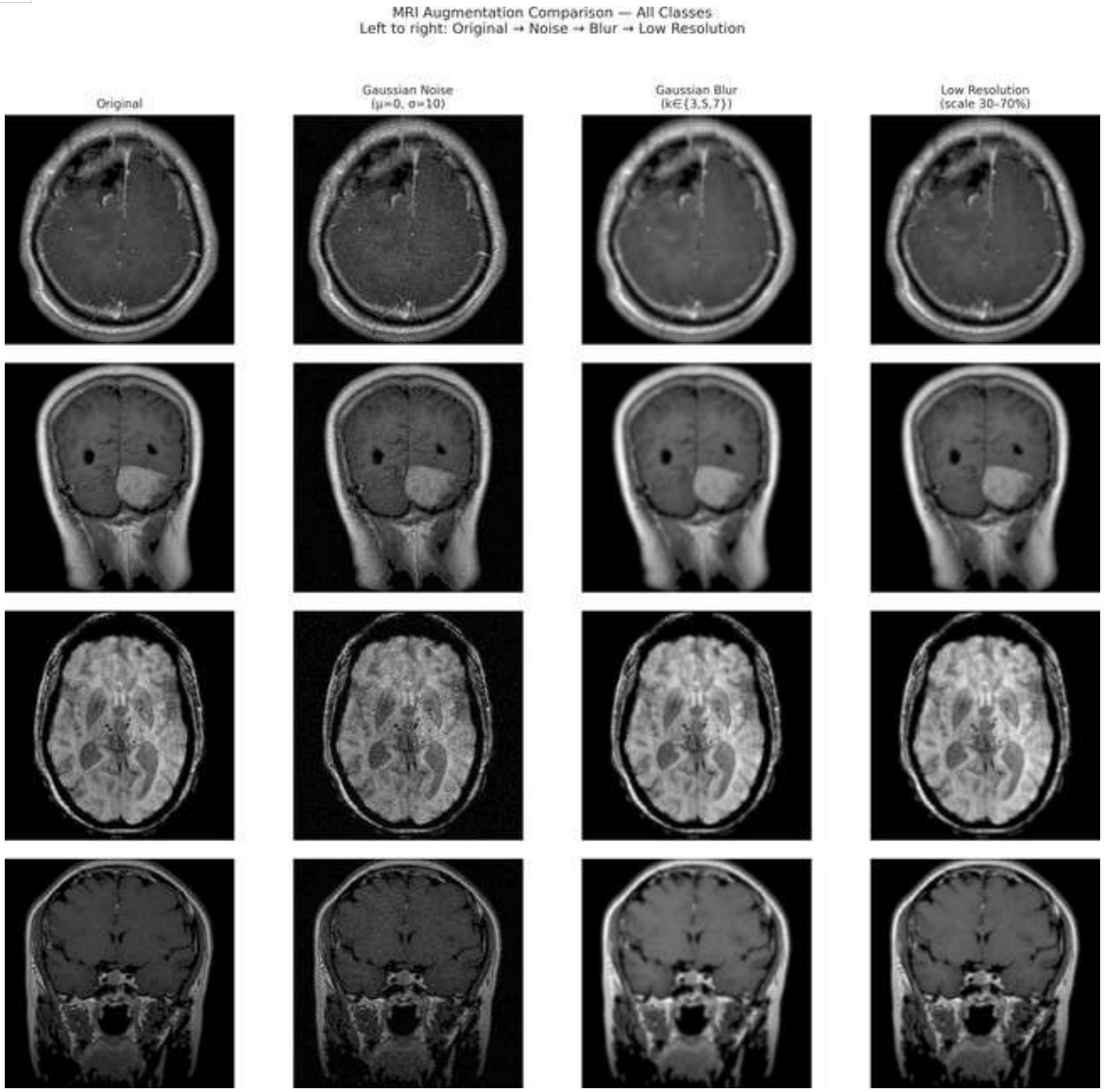

Figure 6:MRI augmentation comparison across all four classes.Columns:original,Gaussiannoise(σ=10),Gaussianblur(k ∈ {3,5,7}),resolutiondegradation(scale30–70%).AllaugmentedsamplesmaintainSSIM ≥0.85.

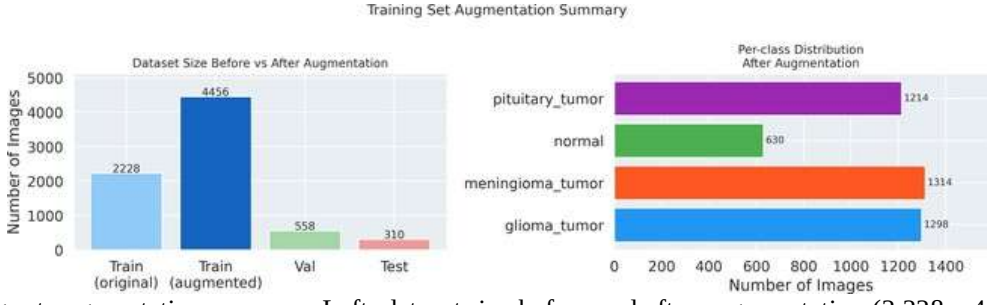

Figure 7: Training set augmentation summary.Left: dataset size before and after aug-mentation (2,228→4,456 images, 2.00× increase).Right:per-class distribution after augmentation.

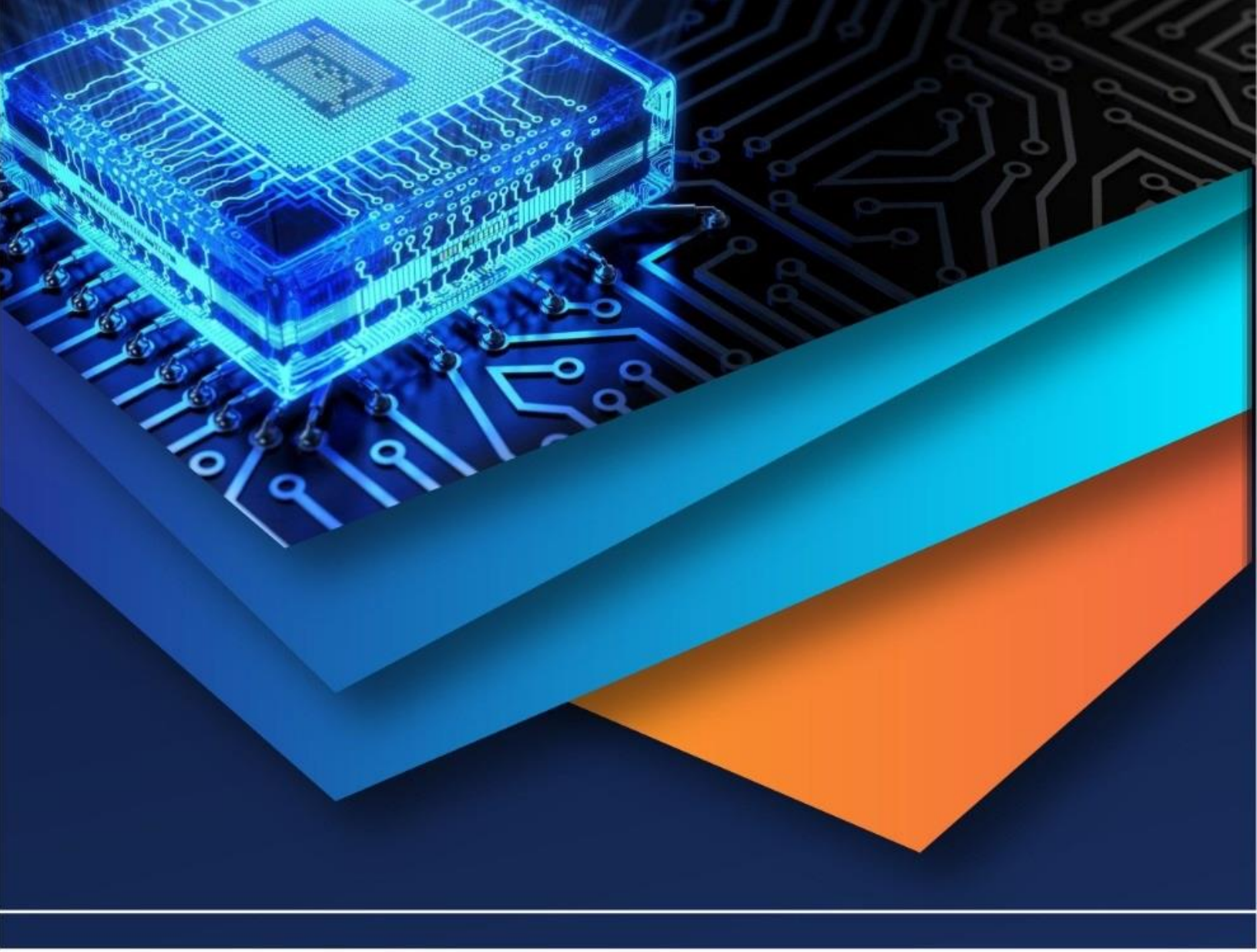

10.22214/IJRASET

45.98

IMPACT FACTOR: 7.129

IMPACT FACTOR: 7.429

INTERNATIONAL JOURNAL FOR RESEARCH

IN APPLIED SCIENCE & ENGINEERING TECHNOLOGY